

# Ridge Structure associated with the Near-Side Jet in the $\Delta\phi$ - $\Delta\eta$ Correlation

Cheuk-Yin Wong

*Physics Division, Oak Ridge National Laboratory, Oak Ridge, TN\* 37831*

(Dated: November 8, 2018)

In the  $\Delta\phi$ - $\Delta\eta$  correlation associated with a near-side jet observed by the STAR Collaboration in heavy-ion collisions at RHIC [Ref. 1-6], the ridge structure can be explained by the momentum kick model in which the ridge particles are identified as medium partons which suffer a collision with the jet and acquire a momentum kick along the jet direction. If this is indeed the correct mechanism, the ridge structure associated with the near-side jet may be used to probe the parton momentum distribution at the moment of the jet-parton collision, leading to the result that at that instant the parton temperature is slightly higher and the rapidity width substantially greater than corresponding quantities of their evolution product inclusive particles at the end point of the nucleus-nucleus collision.

PACS numbers: 25.75.-q 25.75.Dw

## I. INTRODUCTION

Recently, the STAR Collaboration [1, 2, 3, 4, 5, 6] observed a  $\Delta\phi$ - $\Delta\eta$  correlation of particles associated with a jet in RHIC collisions, where  $\Delta\phi$  and  $\Delta\eta$  are respectively the azimuthal angle and pseudorapidity differences measured relative to a trigger jet particle. The experimental measurements, as shown in Fig. 1a and discussed in detail in Refs. [1, 2, 3, 4, 5, 6], reveal the following features of the “ridge phenomenon”:

1. There are particles associated with the trigger jet within a small cone of  $(\Delta\phi, \Delta\eta) \sim (0, 0)$  which belong to the remnants of the near-side jet component. The near-side jet yield is independent of the number of participants.
2. In addition, there are particles associated with the trigger jet within a small range of  $\Delta\phi$  around  $\Delta\phi = 0$  but distributed broadly in  $\Delta\eta$ . These associated particles can be separated as the ridge component associated with the trigger jet.
3. The yield of the ridge component increases approximately linearly with the number of participants and is nearly independent of (i) the flavor content, (ii) the meson/hyperon character, and (iii) the transverse momentum  $p_t$  (above 4 GeV) of the jet trigger [3, 4, 5]. The ridge yield has a temperature that is similar (but slightly higher) than that of the inclusive yield, whereas the near-side jet component has an appreciably higher temperature.

While many theoretical models have been proposed to discuss the jet structure and related phenomena [7, 8, 9, 10, 11, 12, 13], the ridge phenomenon has not yet been fully understood. We would like to propose a simple “momentum kick model” which gives the salient features of the ridge phenomenon. We would also like to discuss the related implications of using the ridge structure to probe the parton momentum distribution at the moment of the jet-parton collision.

This paper is organized as follows. In Section II, we introduce the momentum kick model which involves the momentum kick along the jet direction and the parton momentum distribution at the moment of the jet-parton collision. In Section III, we discuss the parametrization of the initial parton momentum distribution. In Section IV, we examine the effects of the momentum kick and the initial rapidity width on the final momentum distribution after the jet-parton collision. Adopting the hadron-parton duality, we compare the experimental data with momentum kick model results in Section V. In Section VI, we study the ridge structure with identified particles. In Section VII, we examine other predictions of the momentum kick model. In Section VIII, we present the conclusions and discussions.

## II. THE MOMENTUM KICK MODEL

Experimental observation (3) above concerning the properties of the ridge particles implies that these particles are associated with partons in the produced dense medium and much less with (i) the flavor content, (ii) the meson/hyperon character, and (iii) the transverse momentum  $p_t$  (above 4 GeV) of the trigger jet. We are led to such

---

\* wongc@ornl.gov

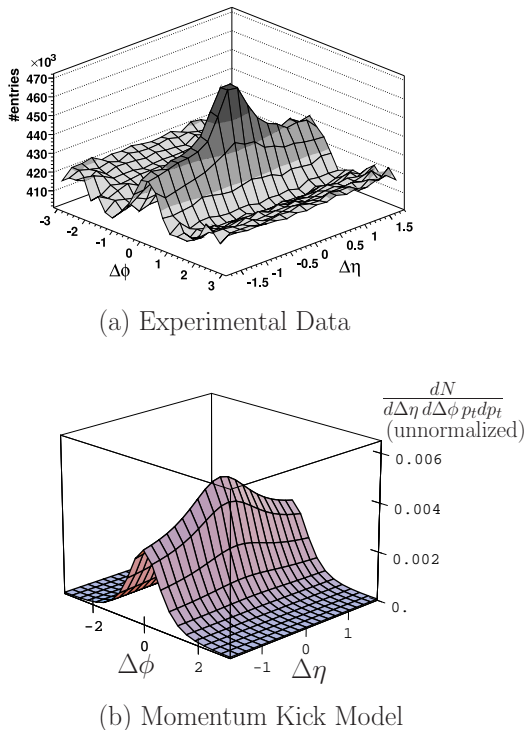


FIG. 1: (a) The experimental yield of associated particles as a function  $\Delta\phi$  and  $\Delta\eta$  [3], showing both the near-side jet at  $(\Delta\phi, \Delta\eta) \sim (0, 0)$  and the ridge structure at  $\Delta\phi \sim 0$  and  $|\Delta\eta| > 0.5$ . (b) The unnormalized yield  $dN/d\Delta\eta d\Delta\phi p_t dp_t$  in the momentum kick model for the description of only the ridge component, calculated for  $p_t = 2$  GeV with  $q = 0.8$  GeV,  $\sigma_y = 5.5$ , and  $T = 0.47$  GeV.

a suggestion of medium partons because the associated ridge particles bear the same “fingerprints” as those of the inclusive particles, including their various particle yields increasing with the participant number and their having nearly similar temperatures. These characteristics suggest that the ridge particles originate from the same material as the produced partons of the dense medium, which later cool down and materialize also as inclusive particles.

Experimental observation (2) above regarding the narrow  $\Delta\phi$  correlation of the ridge particles with the jet implies that these ridge particles of the produced dense medium acquire their azimuthally properties from the jet. The most likely explanation is that these ridge particles are medium partons which suffer a collision with the jet and acquire a momentum kick and the jet’s directionality.

Therefore, to describe the ridge distribution, we propose a simple momentum kick model that incorporates the essential elements of the experimental observations. The momentum kick model contains the following ingredients:

1. A near-side jet occurs near the medium surface and the jet collides with partons in the medium on its way to the detector.
2. The jet-parton collision samples the momentum distribution of the collided medium partons at the moment of the jet-parton collision. Because of the condition for the occurrence of the near-side jet, these collided medium partons are near the surface and each collided parton suffers at most one collision with the jet.
3. The jet-parton collision imparts a momentum kick  $\mathbf{q}$  to the collided parton in the direction of the jet. The momentum kick modifies the parton initial momentum distribution  $P_i(\mathbf{p}_i)$  to turn it into the collided parton final momentum distribution  $P_f(\mathbf{p}_f)$ . After the collided partons hadronize and escape from the surface without further collisions, they materialize as ridge particles which retain the collided parton final momentum distribution.

In mathematical terms, the final momentum distribution of the medium partons which suffer a collision with the jet is,

$$P_f(\mathbf{p}_f) = \int \frac{d\mathbf{p}_i}{E_i} \int d\mathbf{q} P_i(\mathbf{p}_i) P_q(\mathbf{q}) E_f \delta(\mathbf{p}_f - \mathbf{p}_i - \mathbf{q}). \quad (1)$$

By normalizing the momentum kick distribution  $P_q(\mathbf{q})$  as

$$\int d\mathbf{q} P_q(\mathbf{q}) = 1, \quad (2)$$

the kinematic quantities  $E_i$  and  $E_f$  in Eq. (1) ensure the conservation of collided parton numbers before and after the jet-parton collision,

$$N_f = \int \frac{d\mathbf{p}_f}{E_f} P_f(\mathbf{p}_f) = \int \frac{d\mathbf{p}_i}{E_i} P_i(\mathbf{p}_i) = N_i. \quad (3)$$

In the context of the present paper, the initial and final moment distributions  $P_i(\mathbf{p}_i)$  and  $P_f(\mathbf{p}_f)$  refer to the momentum distributions before and after the jet-parton collision respectively, not to be confused with the initial and final momentum distributions at other instants of the nucleus-nucleus collision.

The momentum kick distribution  $P_q(\mathbf{q})$  for the momentum  $\mathbf{q}$  imparted from the jet to a collided medium parton is not a quantity that can be obtained from rigorous first-principles of QCD at present, as many non-perturbative properties of the medium and of the collision process are not known. For the present analysis, of particular interest are the general features of this momentum kick that a collided parton experiences. We know that this momentum kick will be distributed within a narrow cone along the jet direction. While a future refinement to describe this cone distribution is possible, it is illuminating at this stage to introduce as few parameters as possible for the description of this momentum kick, in order to spell out the dominant effects of the jet-parton collision process. Accordingly, we shall use a single parameter  $q$  to describe the momentum kick distribution simply as

$$P_q(\mathbf{q}) = \delta(\mathbf{q} - q\mathbf{e}_{jet}), \quad (4)$$

where  $q = |\mathbf{q}| \geq 0$ , and  $\mathbf{e}_{jet}$  is the unit vector along the jet direction. The simplicity of the model allows us to obtain analytically from Eq. (1) the distribution of partons after suffering a jet-parton collision as

$$\begin{aligned} P_f(\mathbf{p}_f) &= \left[ P_i(\mathbf{p}_i) \frac{E_f}{E_i} \right]_{\mathbf{p}_i = \mathbf{p}_f - q\mathbf{e}_{jet}} \\ &= \left[ P_i(\mathbf{p}_i) \frac{\sqrt{m^2 + p_f^2}}{\sqrt{m^2 + p_i^2}} \right]_{\mathbf{p}_i = \mathbf{p}_f - q\mathbf{e}_{jet}}. \end{aligned} \quad (5)$$

### III. PARAMETRIZATION OF THE PARTON MOMENTUM DISTRIBUTION

In Eq. (5), the initial and final parton momentum distributions can be presented in terms of Cartesian momentum components in the collider frame,  $\mathbf{p} = (p_1, p_2, p_3)$ , with a longitudinal  $p_3$  component, a transverse  $p_1$  component, and a  $p_2$  component perpendicular to both the  $p_1$  axis and the  $p_3$  axis. The coordinate axes can be so chosen that the trigger jet lies in the  $p_1$ - $p_3$  plane. The parton momentum distributions can alternatively be represented in terms of the rapidity  $y$ , the transverse momentum  $\mathbf{p}_t$ , and the azimuthal angle  $\phi$ . They are related to each other. By changing the variables from the Cartesian components  $\mathbf{p}_f = (p_{f1}, p_{f2}, p_{f3})$  to  $(y_f, \phi_f, p_{tf})$ , we have

$$P_f(p_{f1}, p_{f2}, p_{f3}) = \frac{E_f dN_f}{dp_{f1} dp_{f2} dp_{f3}} = \frac{dN_f}{dy_f d\phi_f p_{tf} dp_{tf}}. \quad (6)$$

Similarly, for the initial parton momentum distribution we have

$$P_i(p_{i1}, p_{i2}, p_{i3}) = \frac{dN_i}{dy_i d\phi_i p_{ti} dp_{ti}}. \quad (7)$$

The momentum kick model with a simple delta function momentum kick distribution then gives from Eq. (5)

$$\frac{dN_f}{dy_f d\phi_f p_{tf} dp_{tf}} = \left[ \frac{dN_i}{dy_i d\phi_i p_{ti} dp_{ti}} \frac{E_f}{E_i} \right]_{\mathbf{p}_i = \mathbf{p}_f - q\mathbf{e}_{jet}}. \quad (8)$$

The experimental data are presented not as a rapidity distribution but as a pseudorapidity distribution of the final particles. We need to convert  $dN_f/dy_f\dots$  to  $dN_f/d\eta_f\dots$  [14] and we have

$$\frac{dN_f}{d\eta_f d\phi_f p_{tf} dp_{tf}} = \frac{dN_f}{dy_f d\phi_f p_{tf} dp_{tf}} \sqrt{1 - \frac{m^2}{m_{tf}^2 \cosh^2 y_f}}, \quad (9)$$

where  $m$  is the rest mass of the parton and  $m_{tf} = \sqrt{m^2 + p_{tf}^2}$ .

The above analytical results allow us to evaluate the momentum distribution of the collided partons. We also expect that as the near-side jet occurs near the medium surface, the collided partons also reside near the surface. The energetic collided partons will likely not suffer additional collisions before they hadronize and emerge from the surface as ridge particles. The ridge particles should possess the properties of the energetic collided parton final momentum distribution. We shall therefore assume hadron-parton duality and identify the momentum  $\mathbf{p}$  of the associated particles as the final momentum  $\mathbf{p}_f$  of the energetic partons after the jet-parton collision in Eqs. (8) and (9). This will allow us to identify the distribution  $dN_f/d\eta_f d\phi_f p_{tf} dp_{tf}$  of Eq. (9) as the observed distribution  $dN/d\eta d\phi p_t dp_t$  of associated ridge particles, to be compared with experimental data.

The parton-hadron duality is a reasonable description for the hadronization of energetic partons. We can consider an energetic quark parton [or a  $(\bar{q}\bar{q})_3$  color-triplet cluster parton of two antiquarks] of various flavors and masses. The quark parton [or the  $(\bar{q}\bar{q})_3$  cluster parton] can pick up an antiquark from the sea, which arises spontaneously in a quark-antiquark fluctuation in the medium, and can subsequently emerge out of the medium to become a colorless hadron. Similarly, an energetic antiquark parton [or a  $(qq)_3$  cluster parton of two quarks] can pick up a sea quark and can subsequently emerge as a colorless hadron. On the other hand, an energetic gluon parton can turn itself into a color-octet  $(q\bar{q})_8$  pair which can subsequently emit a soft gluon to become a colorless color-singlet  $(q\bar{q})_1$  quarkonium when it emerges from the medium. For energetic partons, the loss of momentum and energy in picking up a sea quark or antiquark, or emitting a soft gluon, can be approximately neglected. The result is then the (approximate) parton-hadron duality for energetic partons we are considering in the present analysis.

We shall describe the initial momentum distribution of partons on the right-hand side of Eq. (8) by a Gaussian distribution in rapidity  $y_i$  with a width parameter (the standard deviation)  $\sigma_y$ , a thermal transverse momentum distribution characterized by a ‘temperature’  $T$ , and a uniform azimuthal distribution in  $\phi_i$ ,

$$\frac{dN_i}{dy_i d\phi_i p_{ti} dp_{ti}} = A_i e^{-y_i^2/2\sigma_y^2} \frac{\exp\{-\sqrt{m^2 + p_{ti}^2}/T\}}{\sqrt{m^2 + p_{ti}^2}}, \quad (10a)$$

$$A_i = \frac{N_i e^{m/T}}{(2\pi)^{3/2} \sigma_y T}, \quad (10b)$$

where  $N_i$  is a total number of partons that collide with the jet. Note that the ‘initial parton temperature’  $T$  has been introduced using the above form of the transverse momentum distribution. This functional form has been chosen to give a simple description of the experimental central collision inclusive transverse momentum spectrum from 0.2 GeV to  $\sim 4$  GeV, characterized by an inclusive ‘temperature’  $T_{incl} = 0.40$  GeV [see Fig. 5(a) below]. To be consistent, we expect the initial parton temperature  $T$  introduced here to be higher than the temperature  $T_{incl}$  of inclusive particles, as the initial partons will presumably cool down and evolve to become the inclusive particles at the end-point of parton evolution.

For a trigger jet with a transverse momentum  $p_{tjet}$  at a pseudorapidity  $\eta_{jet}$ , we have

$$|\mathbf{p}_{jet}| = p_{tjet} \cosh \eta_{jet}, \quad (11)$$

and

$$p_{3jet} = p_{tjet} \sinh \eta_{jet}. \quad (12)$$

As a consequence, the unit vector along the jet direction is

$$\mathbf{e}_{jet} = \frac{\mathbf{e}_1 + \sinh \eta_{jet} \mathbf{e}_3}{\cosh \eta_{jet}}, \quad (13)$$

where  $\mathbf{e}_1$  and  $\mathbf{e}_3$  are unit vectors along the  $p_1$  and  $p_3$  directions, respectively. The final momentum distribution is therefore

$$\frac{dN_f}{d\eta_f d\phi_f p_{tf} dp_{tf}} = \left[ A_i e^{-y_i^2/2\sigma_y^2} \frac{e^{-m_{ti}/T}}{m_{ti}} \frac{E_f}{E_i} \right]_{\mathbf{p}_i = \mathbf{p}_f - q \mathbf{e}_{jet}} \sqrt{1 - \frac{m^2}{m_{tf}^2 \cosh^2 y_f}}, \quad (14)$$

where the initial momentum  $\mathbf{p}_i = (p_{i1}, p_{i2}, p_{i3})$  is related to the final momentum  $\mathbf{p}_f = (p_{f1}, p_{f2}, p_{f3})$  and the trigger jet rapidity  $\eta_{jet}$  by

$$p_{i1} = p_{f1} - \frac{q}{\cosh \eta_{jet}}, \quad (15a)$$

$$p_{i2} = p_{f2}, \quad (15b)$$

$$p_{i3} = p_{f3} - \frac{q \sinh \eta_{jet}}{\cosh \eta_{jet}}, \quad (15c)$$

and  $y_i$  and  $m_{ti}$  are the initial rapidity and transverse mass

$$y_i = \frac{1}{2} \ln \frac{E_i + p_{i3}}{E_i - p_{i3}}, \quad (16)$$

$$m_{ti} = \sqrt{m^2 + p_{i1}^2 + p_{i2}^2}. \quad (17)$$

The number of partons that collide with the jet  $N_i$  is an overall normalization constant. At this stage, we shall examine “unnormalized” distributions  $dN/d\Delta\eta d\Delta\phi p_t dp_t$  with  $N_i$  set to 1 in Figs. 1, 2, 3, and 8, so that the results can be rescaled when normalized experimental data are available. For numerical purposes, we take  $m = m_\pi$ , the mass of the pion, unless indicated otherwise.

#### IV. DEPENDENCE OF THE RIDGE STRUCTURE ON THE MOMENTUM KICK AND THE RAPIDITY WIDTH

Experimental data are presented in terms of  $\Delta\eta = \eta - \eta_{jet}$  and  $\Delta\phi = \phi - \phi_{jet}$ , relative to the trigger jet  $\eta_{jet}$  and  $\phi_{jet}$ . We can obtain  $dN/d\Delta\eta d\Delta\phi p_t dp_t$  relative to the jet pseudorapidity and azimuthal angle from  $dN/d\eta d\phi p_t dp_t$  by a simple change of variables. For such a purpose, we need the experimental pseudorapidity distribution of the trigger jet in STAR measurements, [16]

$$\frac{dN_{jet}}{d\eta_{jet}} = \frac{\Theta(0.85 - |\eta_{jet}|)}{1.7}. \quad (18)$$

We shall see in the next section that a reasonable set of parameters that can reproduce the main features of the experimental data are  $q = 0.8$  GeV,  $\sigma_y = 5.5$ , and  $T = 0.47$  GeV. To examine the effects of the the momentum kick and the initial parton momentum distribution on the  $\Delta\phi$ - $\Delta\eta$  correlation, we shall vary one of the three parameters of  $\{q, \sigma_y, T\}$  in this set, with the remaining two parameters being held fixed.

We show in Fig. 2 the unnormalized yield  $dN/d\Delta\eta d\Delta\phi p_t dp_t$  of ridge particles at  $p_t = 2$  GeV obtained in the momentum kick model for different values of  $q$ . Figs. 2(a), 2(b), and 2(c) are for  $q = 0, 0.4,$  and  $0.8$  GeV respectively, the other parameters being fixed as  $\sigma_y = 5.5$  and  $T = 0.47$  GeV. They are calculated with  $N_i = 1$  in Eqs. (10a) and (10b) for  $p_t = 2$  GeV. As one observes in Fig. 2(a), when the momentum kick is zero the distribution is essentially flat in  $\Delta\phi$  and  $\Delta\eta$ . [There is a small variation of the distribution along the  $\Delta\eta$  direction, but with  $\sigma_y = 5.5$ , the variation is too small to show up in Fig. 2(a).] When there is a non-zero momentum kick, the distribution develops a peak at  $\Delta\phi = 0$  and a ridge along the  $\Delta\eta$  direction. The height of the peak increases and its width decreases, as the magnitude of  $q$  increases.

It is easy to understand how a peak structure at  $\Delta\phi = 0$  along the  $\Delta\phi$  direction arises in the momentum kick model. Consider a parton with a final momentum  $\mathbf{p}_f = (\eta_f, \Delta\phi, p_{tf})$  at a fixed pseudorapidity  $\eta_f$  and transverse momentum  $p_{tf}$  with various azimuthal angles  $\Delta\phi$ . Under the action of a momentum kick along the jet direction, the square of the magnitude of the initial parton transverse momentum  $p_{ti}^2$  is related to the final transverse momentum  $p_{tf}$  by

$$p_{ti}^2 = p_{tf}^2 - 2p_{tf} q \cos \Delta\phi / \cosh \eta_{jet} + q^2 / \cosh^2 \eta_{jet} \quad (19)$$

The magnitude of the initial transverse momentum  $p_{ti}$  is a minimum at  $\Delta\phi = 0$ , and it increases monotonically as  $\Delta\phi$  increase to  $\pi$ . Because the initial transverse momentum  $p_{ti}$  is distributed according to  $\exp\{-\sqrt{m^2 + p_{ti}^2}/T\}/\sqrt{m^2 + p_{ti}^2}$ , the probability distribution decreases for increasing  $p_{ti}$ . Thus, there are more collided partons at  $\Delta\phi = 0$  than at  $\Delta\phi = \pi$ , for the same observed final transverse momentum  $p_{tf}$ . The case of

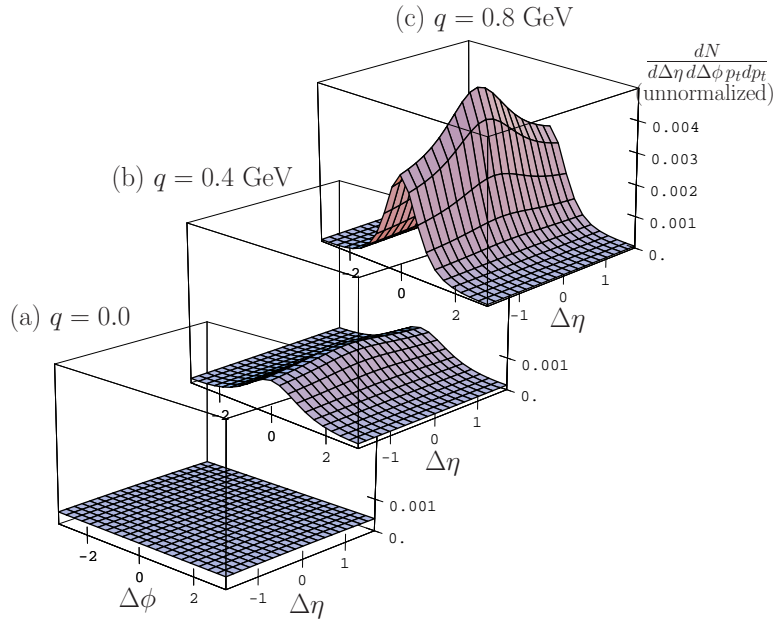


FIG. 2: The results of the momentum kick model for the unnormalized yield  $dN/d\Delta\eta d\Delta\phi p_t dp_t$  of associated ridge particles at  $p_t = 2$  GeV, as a function  $\Delta\phi$  and  $\Delta\eta$ . Figs. 2(a), 2(b), and 2(c) are for  $q = 0, 0.4, \text{ and } 0.8$  GeV respectively.

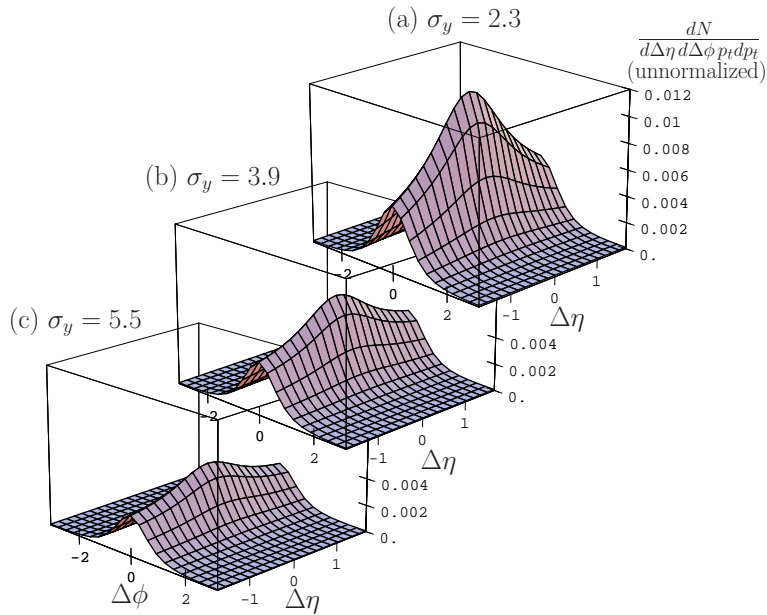


FIG. 3: The results of the momentum kick model for the unnormalized yield  $dN/d\Delta\eta d\Delta\phi p_t dp_t$  of associated particles at  $p_t = 2$  GeV as a function  $\Delta\phi$  and  $\Delta\eta$ . Figs. 3(a), 3(b), and 3(c) are for  $\sigma_y = 2.3, 3.9, \text{ and } 5.5$  respectively.

azimuthal angles between  $\Delta\phi = 0$  and  $\Delta\phi = \pi$  gives a momentum distribution in between these two limits, resulting in a peak structure in  $\Delta\phi$  centered at  $\Delta\phi = 0$ . The height of the peak increases and its width decreases, as  $q$  increases.

While the narrow peak as a function of  $\Delta\phi$  depends mainly on the momentum kick  $q$ , the ridge structure along the  $\Delta\eta$  direction depends mainly on the initial rapidity distribution. The rapidity distribution of inclusive experimental data for central Au-Au collisions at  $\sqrt{s_{NN}} = 200$  GeV can be well described by a Gaussian distribution with a rapidity width parameter of  $\sigma_y = 2.3$  which agrees with the Landau hydrodynamics prediction of  $\sigma_y = 2.16$  within 5% [15].

We would like to see whether the ridge structure associated with the near-side jet can be described by such a rapidity width parameter. We would also like to see how the ridge structure depends on the rapidity width parameter  $\sigma_y$ .

Accordingly, we carry out calculations in the momentum kick model for  $\sigma_y = 2.3, 3.9,$  and  $5.5$  and the results of the unnormalized yield  $dN/d\Delta\eta d\Delta\phi p_t dp_t$  are shown in Figs. 3(a), 3(b) and 3(c) respectively. In these calculations, the other parameters are kept fixed as  $q = 0.8$  GeV and  $T = 0.47$  GeV, and the results are obtained for  $p_t = 2$  GeV.

As one observes in Fig. 3(a), the distribution  $dN/d\Delta\eta d\Delta\phi p_t dp_t$  for  $\sigma_y = 2.3$  has a ridge with a steep slope toward the maximum peak along the  $\Delta\eta$  direction at  $\Delta\phi = 0$ . The slope of the ridge appears to be too steep compared to the experimental data (see also Fig. 4(b) below), when the distribution is matched with the magnitude of the experimental data. Apparently, the width parameter that describes the inclusive rapidity distribution data cannot reproduce the ridge structure associated with the jet.

The ridge becomes broader along the  $\Delta\eta$  direction as  $\sigma_y$  increases. When we increase the ridge width parameter to  $\sigma_y = 3.9$  and  $\sigma_y = 5.5$ , the slope of the ridge becomes less steep as shown in Figs. 3(b) and 3(c).

## V. COMPARISON OF THE MODEL WITH EXPERIMENTAL DATA

We compare the momentum kick model results with the experimental data [3] at specific cuts in  $\Delta\eta$  or  $\Delta\phi$  in Fig. 4 and with the two-dimensional  $\Delta\phi$ - $\Delta\eta$  distribution in Fig. 1. The experimental data contain both the near-side jet and the ridge component, in addition to other unknown contributions at  $|\Delta\phi| > 1$ . The near-side jet component shows up as a peak at  $(\Delta\phi, \Delta\eta) \sim (0, 0)$ , and the ridge component at  $\Delta\phi \sim 0$  with a relatively flat ridge along the  $\Delta\eta$  direction.

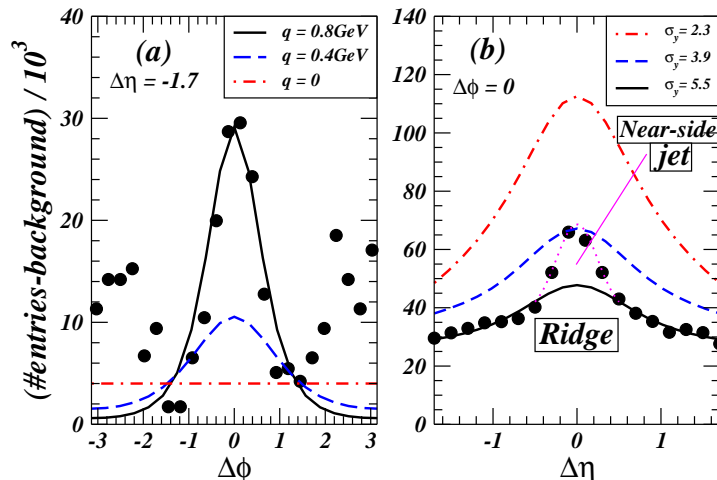


FIG. 4: The unnormalized experimental associated particle data [3] shown as solid circular points, compared with the solid curves calculated in the momentum kick model for  $p_t = 2$  GeV with  $q = 0.8$  GeV,  $\sigma_y = 5.5$  and  $T = 0.47$  GeV. The solid curves are normalized by matching theoretical results with the experimental data at  $(\Delta\phi, \Delta\eta) = (0, -1.7)$ . Fig. 4(a) gives  $dN/d\Delta\eta d\Delta\phi p_t dp_t$  as a function of  $\Delta\phi$  at  $\Delta\eta = -1.7$ . Fig. 4(b) gives  $dN/d\Delta\eta d\Delta\phi p_t dp_t$  as a function of  $\Delta\eta$  at  $\Delta\phi = 0$ . The dashed, and dash-dot curves are the momentum kick model results by varying  $q$  in Fig. 4(a), and varying  $\sigma_y$  in Fig. 4(b).

As the ridge component has not been cleanly separated, we shall be content at this stage with a qualitative analysis to compare the results of the momentum kick model only with the ridge portion of the experimental data [3], without considering the near-side peak at  $(\Delta\phi, \Delta\eta) \sim (0, 0)$  and other contributions with  $|\Delta\phi| > 1$ .

We find that the ‘best-fit’ set of parameters  $q = 0.8$  GeV,  $\sigma_y = 5.5$ , and  $T = 0.47$  GeV gives a reasonable qualitative description of the ridge component of the experimental data, as shown by the solid curves in Figs. 4(a) and 4(b). In these comparisons, the theoretical calculations are normalized by matching the experimental distribution [3] at the point  $(\Delta\phi, \Delta\eta) = (0, -1.7)$  with the momentum kick model result calculated with the set of parameters  $q = 0.8$  GeV,  $\sigma_y = 5.5$ , and  $T = 0.47$  GeV. The experimental data points are taken from Ref. [3] and shown in Figs. 1(a) and 4. The experimental background is taken to be  $405 \times 10^3$  entries such that the lowest data point, at  $(\Delta\phi, \Delta\eta) = (1.2, -1.7)$ , is nearly at the background level. The data in Fig. 4 have not been corrected for  $v_2$  elliptic flow. The  $v_2$  corrections involves the product of  $v_2(\text{jet}) \sim 0.1$  and the  $v_2(\text{associated particles}) \sim 0.05$  and will probably modified the resultant parameters only slightly. It will be of interest to readjust the parameters when the  $v_2$ -corrected data become available.

We study the variation of shape of the ridge structure as a function of  $q$  at  $\Delta\eta = -1.7$  in Fig. 4(a), and separately as a function of  $\sigma_y$  at  $\Delta\phi = 0$  in Fig. 4(b). We calculate the yield  $dN/d\Delta\eta d\Delta\phi p_t dp_t$  at  $p_t = 2$  GeV for values

of  $q$  and  $\sigma_y$  different from those in the best-fit set, using the same normalization as used for the best-fit set. The results of using parameters different from the best-fit set are shown as the dashed and dash-dot curves in Figs. 4(a) and 4(b). One notes that many features of the theoretical results of these dashed and dash-dot curves do not match those of the experimental data. For example, in Fig. 4(a) for  $q = 0.4$  GeV, the full width at half maximum is about  $\Delta\phi \sim 2.4$  which is much greater than the experimental full width at half maximum of about  $\Delta\phi \sim 1.2$ . In Fig. 4(b) for  $\sigma_y = 2.3$ , the ridge yield increase by a factor of about 1.7 when  $\Delta\eta$  increases from -1.7 to -0.7, whereas the experimental data shows an increase of only a factor of about 1.2. In contrast, the solid curves obtained with the best-fit set of parameters,  $q = 0.8$  GeV,  $\sigma_y = 5.5$ , and  $T = 0.47$  GeV, give a good representation of the ridge data.

To compare the two-dimensional distributions, we plot in Fig. 1(a) the experimental yield [3] and in 1(b) the unnormalized yield  $dN/d\Delta\eta d\Delta\phi p_t dp_t$  in the momentum kick model, as a function of both  $\Delta\phi$  and  $\Delta\eta$ , at  $p_t = 2$  GeV using our best-fit set of parameters,  $q = 0.8$  GeV,  $\sigma_y = 5.5$ , and  $T = 0.47$  GeV. The general two-dimensional features of the ridge are qualitatively reproduced. A more careful quantitative analysis of the ridge structure will need to await quantitative data in which the ridge component can be cleanly separated. Ridge measurements extending to greater values of  $|\eta|$  will also be of great interest in determining more accurately the rapidity width parameter  $\sigma_y$  and finding out whether the initial rapidity distribution may be non-Gaussian at the moment of the jet-parton collision.

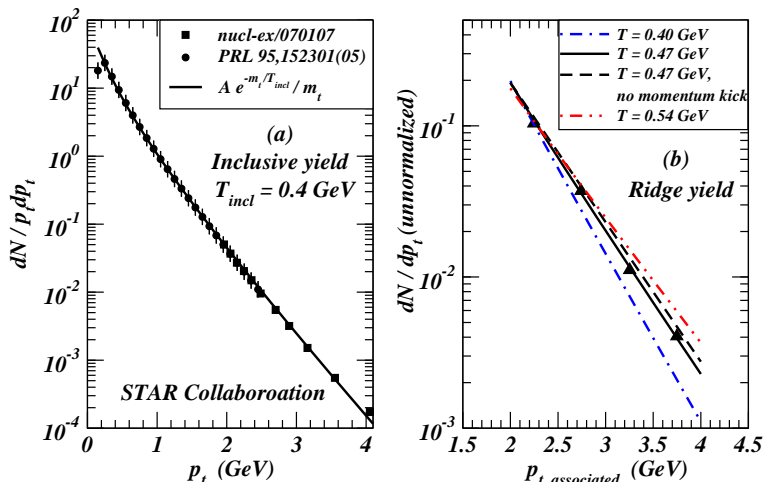


FIG. 5: The central collision transverse momentum distributions of (a) inclusive particles and (b) ridge particles. The solid curve in (a) is the theoretical distribution of  $dN/p_t dp_t \propto \exp\{-m_t/T_{incl}\}/m_t$  with  $T_{incl} = 0.40$  GeV, and the data points are from Refs. [1] and [3]. In Fig. 5(b), the data points are experimental ridge yield (proportional to  $dN/dp_t$ ) [3]. The dash-dot, solid, and dash-dot-dot curves are the  $dN/dp_t$  results of the momentum kick model for  $T = 0.50, 0.47, 0.40$  GeV, respectively. They are calculated with  $q = 0.8$  GeV and  $\sigma_y = 5.5$  and normalized to match the data point at  $p_{t,assoc} = 2.13$  GeV. The dashed curve is theoretical results of  $dN/dp_t \propto p_t \exp\{-m_t/T_{incl}\}/m_t$  with  $T = 0.47$  GeV and no momentum kick.

We can now examine the transverse momentum distribution of the ridge particles. We show in Fig. 5(a) and 5(b) the transverse distribution data of inclusive particles [1] and ridge particles [3] respectively, together with theoretical fits. The inclusive  $dN/p_t dp_t$  data in Fig. 5(a) can be described by a distribution of the form  $A \exp\{-m_t/T_{incl}\}/m_t$  with an inclusive ‘temperature’ parameter  $T_{incl} = 0.40$  GeV. The ridge particle yield calculated in the momentum kick model for different values of  $T$  are given in Fig. 5(b) and compared with the experimental transverse yield (proportional to  $dN/dp_t$ ) for a jet trigger of  $4 \text{ GeV} < p_{trig} < 5 \text{ GeV}$  [3]. In this comparison, we have normalized the results from the momentum kick model by matching the theoretical  $dN/dp_t$  results with the experimental data point at  $p_{t,associated} = 2.13$  GeV. The transverse momentum distribution from the momentum kick model with  $T = 0.47$  GeV, represented by the solid curve, agrees well with data, whereas the results from  $T = 0.40$  GeV and  $T = 0.54$  GeV given by the dash-dot and dash-dot-dot curves do not agree with the ridge transverse distribution. As a further comparison, we show also the theoretical transverse momentum distribution  $dN/dp_t \propto p_t \exp\{-(m_t - m)/T\}/m_t$  with  $T = 0.47$  GeV without the momentum kick as the dashed curve. Comparison of the solid and the dashed curves indicates that the shape of the transverse momentum distribution in this  $p_t$  region is changed only very slightly by the presence of the momentum kick  $q$ .

The results of Fig. 5(a) and 5(b) indicate that the parton medium at the moment of jet-parton collision has a temperature higher than the temperature of the inclusive particles at the end point of parton evolution, as noted earlier in a different parametrization of the transverse momentum distribution [3, 4, 5].



## VI. STUDY OF THE RIDGE STRUCTURE WITH IDENTIFIED PARTICLES

Recent measurements with identified trigger particles [4] and identified ridge particles [5] provide useful information on the ridge phenomenon. The gross structure of the ridge is nearly unaffected by the flavor, the meson/hyperon character, and the transverse momentum (above 4 GeV) of the trigger jet. This implies that (i) the parton-jet interaction is approximately independent of the jet structure, and (ii) the momentum kick  $q$  suffered by the parton in a jet-parton collision is, to the lowest order, a constant quantity. Finer dependencies of  $q$  on the invariant mass and flavor of the jet trigger are possible and may be explored by future accurate measurements.

We shall first present some general results concerning the ratio of local yields at a specific transverse momentum  $p_t$  for identified associated ridge particles within the momentum kick model. Specifically, for two parton species with parton masses  $m_1$  and  $m_2$  with parton numbers  $N_1$  and  $N_2$ , the momentum kick model gives the final ratio at  $p_t$

$$R_{m_1/m_2}(p_t) = \frac{dN_1/p_t dp_t(m_1, p_t)}{dN_2/p_t dp_t(m_2, p_t)} \sim \frac{dN_1^{(\text{init})}/p_t dp_t(m_1, |p_t - q|)}{dN_2^{(\text{init})}/p_t dp_t(m_2, |p_t - q|)} = R_{m_1/m_2}^{(\text{init})}(|p_t - q|), \quad (20)$$

relating the observed ratio of the species at  $p_t$  to the ratio of the initial parton distributions at a lower momentum,  $|p_t - q|$ , displaced by the momentum kick  $q$ . If the  $m_t$  scaling of the initial parton distribution in the form of Eq. (10) is a good description, then the initial transverse momentum distribution ratio is given by

$$\begin{aligned} R_{m_1/m_2}(p_t) &\sim \frac{dN_1^{(\text{init})}/p_t dp_t(m_1, |p_t - q|)}{dN_2^{(\text{init})}/p_t dp_t(m_2, |p_t - q|)} \\ &= \frac{N_1 e^{m_1/T} \sqrt{m_2^2 + (p_t - q)^2} \exp\{-\sqrt{m_1^2 + (p_t - q)^2}/T\}}{N_2 e^{m_2/T} \sqrt{m_1^2 + (p_t - q)^2} \exp\{-\sqrt{m_2^2 + (p_t - q)^2}/T\}}. \end{aligned} \quad (21)$$

For  $p_t \gg m_1, m_2$ ,

$$R_{m_1/m_2}(p_t) \sim \frac{N_1}{N_2} e^{(m_1 - m_2)/T}, \quad (22)$$

which is independent of  $p_t$ . For  $|p_t - q| \rightarrow 0$  (if the model remains valid),

$$R_{m_1/m_2}(p_t) \sim \frac{N_1 m_2}{N_2 m_1}. \quad (23)$$

It will be of interest to examine how these results can be confronted with experimental measurements of different species among the ridge particles.

In the experiments performed by the STAR Collaboration, the ratio of the yield of various identified particles have been obtained not at a single  $p_t$  but over a range of  $p_t$  with trigger particles spanning over a range of transverse momenta. Specifically, the experimental  $\Lambda/K_s^0$  ratio was obtained for Au on Au at  $\sqrt{s_{NN}} = 200$  GeV at 0-10% centrality, within the kinematic domain specified by [5]

$$\begin{aligned} p_{tjet,min} &= 2 \text{ GeV}, \quad p_{tjet,max} = 3 \text{ GeV}, \\ \text{and identified ridge particles with } p_{tmin} &= 1.5 \text{ GeV} < p_t < p_{tjet}. \end{aligned} \quad (24)$$

In the momentum kick model, the ratio of the ridge particles within the kinematic domain (24) as defined by the measurement is given by

$$\langle R_{\Lambda/K_s^0} \rangle_{\text{ridge}} = \frac{\int_{p_{tjet,min}}^{p_{tjet,max}} P_{jet}(p_{tjet}) p_{tjet} dp_{tjet} \int_{p_{tmin}}^{p_{tjet}} P_{\Lambda}(p_t - q) p_t dp_t}{\int_{p_{tjet,min}}^{p_{tjet,max}} P_{jet}(p_{tjet}) p_{tjet} dp_{tjet} \int_{p_{tmin}}^{p_{tjet}} P_{K_s^0}(p_t - q) p_t dp_t}. \quad (25)$$

We shall use hadron-parton duality and assume the equivalence of the hadron mass and the parton mass. The transverse momentum distribution of the  $\lambda$ -type species in the above equation is given by

$$P_{\lambda}(p_t) = \frac{dN_{\lambda}}{p_t dp_t}(p_t) = \frac{N_{\lambda} \exp\{-(\sqrt{p_t^2 + m_{\lambda}^2} - m_{\lambda})/T\}}{\sqrt{p_t^2 + m_{\lambda}^2}}, \quad (26)$$

where  $N_{\lambda}$  is the total number of the produced  $\lambda$ -type parton in the medium,

$$N_{\lambda} = \int \frac{dN_{\lambda}}{p_t dp_t}(p_t) p_t dp_t, \quad (27)$$

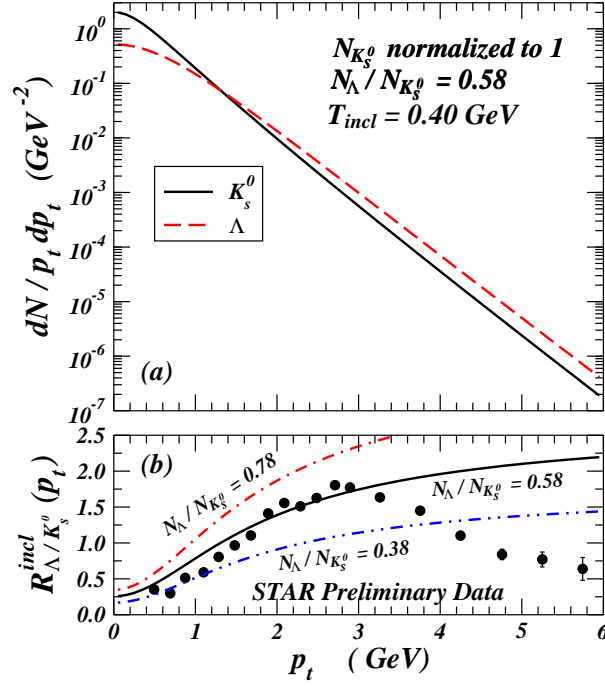


FIG. 6: (a) Theoretical transverse momentum distributions of inclusive  $K_s^0$  and  $\Lambda$  particles based on the distribution Eq. (30) with  $N_{K_s^0}$  normalized to 1,  $N_{\Lambda}/N_{K_s^0} = 0.58$ , and  $T_{inclusive} = 0.40$  GeV. Fig. 6(b) gives the ratio of inclusive  $R_{\Lambda/K_s^0}^{incl}(p_t)$  as a function of  $p_t$ . The dash-dot, solid, and dash-dot-dot curves are the theoretical ratio  $R_{\Lambda/K_s^0}^{incl}(p_t)$  calculated with  $N_{\Lambda}/N_{K_s^0} = 0.78$ , 0.58, and 0.38, respectively. The experimental data points are from Ref. [5].

and  $T$  is the initial parton temperature at the moment of jet-parton collision,  $T = 0.47$  GeV. For the jet trigger transverse momentum distribution, we can use the experimental distribution

$$\frac{dP}{p_{tjet} dp_{tjet}} \propto \exp\{-p_{tjet}/T_{jet}\} \quad (28)$$

with  $T_{jet} = 0.478$  GeV for hadron jet triggers [5]. [Note that  $T_{jet}$  pertains to the above form of  $p_{tjet}$  distribution [5], which differs from our form of the  $p_t$  distribution, Eq. (26), for initial partons.]

For the evaluation of the  $\langle R_{\Lambda/K_s^0} \rangle_{ridge}$  as given by Eqs. (25) and (26), we need to know the ratio of total parton numbers,  $N_{\Lambda}/N_K$ , in the parton medium. We can infer such a ratio from the inclusive data where we have

$$R_{\Lambda/K_s^0}^{incl}(p_t) = \frac{dN_{\Lambda}^{incl}/p_t dp_t(m_{\Lambda}, p_t)}{dN_{K_s^0}^{incl}/p_t dp_t(m_{K_s^0}, p_t)}, \quad (29)$$

and the inclusive yield is

$$\frac{dN_{\lambda}^{incl}}{p_t dp_t}(m_{\lambda}, p_t) = \frac{N_{\lambda} \exp\{-\sqrt{m_{\lambda}^2 + p_t^2}/T_{incl}\}}{\sqrt{m_{\lambda}^2 + p_t^2}}. \quad (30)$$

The inclusive temperature parameter appropriate for the medium at the end point of the parton evolution has been determined from Fig. 5(a) to be  $T_{incl} = 0.40$  GeV. In Fig. 6(a), we show the transverse distributions of  $K_s^0$  and  $\Lambda$ , normalized to  $N_{K_s^0} = 1$  and  $N_{\Lambda}/N_{K_s^0} = 0.58$ . By taking the ratio of the two types of particles at different transverse momenta in Fig. 6(a), we obtain solid curve of  $R_{\Lambda/K_s^0}^{incl}(p_t)$  in Fig. 6(b). We also calculate  $R_{\Lambda/K_s^0}^{incl}(p_t)$  for the ratios of  $N_{\Lambda}/N_{K_s^0} = 0.38$  and 0.78, shown as the dash-dot and dash-dot-dot curves in Fig. 6(b). Comparison of  $R_{\Lambda/K_s^0}^{incl}(p_t)$  experimental data points with the three different predictions using different  $N_{\Lambda}/N_{K_s^0}$  ratios indicates that  $N_{\Lambda}/N_{K_s^0} = 0.58$  gives a good description of the experimental inclusive ratio  $R_{\Lambda/K_s^0}^{incl}(p_t)$  for  $p_t < 3$  GeV. The region of  $p_t > 3$  GeV involves additional fragmentation mechanisms for baryon and meson production, and cannot be described by the above equation of  $m_t$  scaling. Fortunately, the kinematic domain of interest lies in the region of  $p_t < 3$  GeV.

Carrying out the integrations in Eq. (25) and using the total parton numbers ratio  $N_\Lambda/N_{K_s^0} = 0.58$  determined from inclusive data of Fig. 6(b), we obtain  $\langle R_{\Lambda/K_s^0} \rangle_{ridge} = 0.71$  within the kinematic domain specified by Eq. (24). Within the experimental error, this theoretical ratio for ridge particle in the momentum kick model is consistent with the observed measurement of  $\langle R_{\Lambda/K_s^0} \rangle_{ridge} = 0.81 \pm 0.14$ . The corresponding value for the jet is  $0.46 \pm 0.21$ , which is smaller than  $\langle R_{\Lambda/K_s^0} \rangle_{ridge}$ .

## VII. OTHER PREDICTIONS OF THE MOMENTUM KICK MODEL

The momentum kick model is based on simplifying idealizations. The model needs to be tested and improved by comparing its predictions with experimental measurements.

We have assumed that the initial rapidity distribution is in the form of a Gaussian distribution with a standard deviation  $\sigma_y$ . A distribution with  $\sigma_y = 5.5$  appears to give a good description of the measured ridge pseudorapidity data up to  $|\Delta\eta| < 1.7$ . It is also possible that the shape of the initial rapidity distribution may be non-Gaussian or multi-center in nature. It is therefore useful to obtain the predicted distribution at large pseudorapidity, for a Gaussian initial rapidity distribution.

For definiteness, we take the trigger jet distribution as given by Eq. (18), corresponding to the experimental jet acceptance of the STAR Collaboration around  $\eta_{jet} \sim 0$ . We calculate the pseudorapidity distribution of the associated particles for this trigger jet distribution. The solid curves in Figure 7 shows the predictions from the momentum kick model for  $q = 0.8$  GeV,  $\sigma_y = 5.5$ , and  $T = 0.47$  GeV, calculated for  $p_t = 2$  GeV. The fall-off of the ridge distribution is gradual and has a slope different from that in the smaller  $\Delta\eta$  region around  $\Delta\eta \sim 0$ . The decrease is rather slow as a function of  $\Delta\eta$ , decreasing by about 30% as  $\Delta\eta$  changes from  $\Delta\eta = 1.7$  to  $\Delta\eta = 5$ .

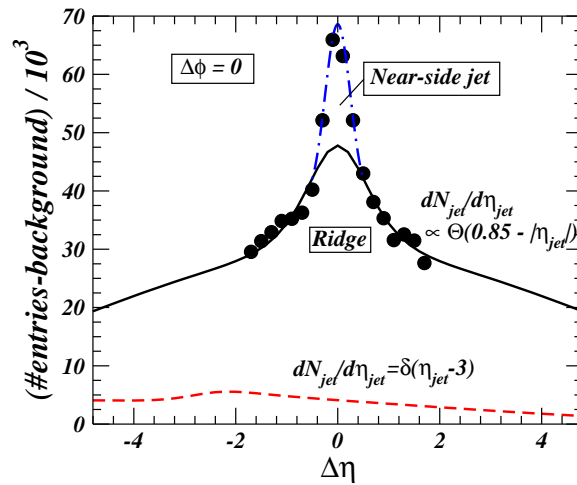


FIG. 7: The yield  $dN/d\Delta\eta d\Delta\phi p_t dp_t$  obtained in the momentum kick model for the description of only the ridge component, calculated for  $p_t = 2$  GeV with  $q = 0.8$  GeV,  $\sigma_y = 5.5$ , and  $T = 0.47$  GeV, normalized to the yield at  $\Delta\eta = -1.7$ . The solid curve is for  $dN_{jet}/d\eta_{jet} = \Theta(0.85 - |\eta_{jet}|)/1.7$  and the dashed curve is for  $dN_{jet}/d\eta_{jet} = \delta(\eta_{jet} - 3)$

Previously, STAR has attempted to measure the associated particles at forward rapidities. They indeed observed a hint of the ridge effect at forward rapidity although the systematic uncertainty is large [17, 18]. It will be of great interest to make a quantitative comparison so as to probe the initial rapidity distribution in the forward region.

Another interesting question is to inquire what kind of associated particle distribution will be expected for a forward jet trigger, say, at  $\eta_{jet} = 3$ . The dashed curve in Fig. 6 shows the pseudorapidity distribution of the associated particles as a function of the pseudorapidity relative to the jet pseudorapidity for  $\eta_{jet} = 3$ . We observe that the peak of the  $dN/d\Delta\eta$  distribution of the associated particle is shifted and is located at  $\Delta\eta \sim -2.2$  (corresponding to  $\eta_{Lab} \sim 0.8$ ). The shape of the distribution is not symmetrical with respect to the peak and the magnitude of the distribution at the peak is small compared with that for the case with the jet trigger at  $\eta_{jet} \sim 0$ .

Figure 8 shows the 3-D associated particle distribution for a trigger jet with  $\eta_{jet} = 3$ , calculated for  $p_t = 2$  GeV with  $q = 0.8$  GeV,  $\sigma_y = 5.5$ , and  $T = 0.47$  GeV. We observe that the ridge is now not in the  $\Delta\eta$  direction as in the case of jet trigger  $\eta \sim 0$  case, but in the  $\Delta\phi$  direction. The peak of the ridge is shifted and located at  $\Delta\eta \sim -2.2$ , as mentioned previously. Although the collided parton gains a momentum kick along the jet direction, the pseudorapidity of the peak is not at  $\Delta\eta = 0$ . It is shifted and appears at  $\Delta\eta \sim -2.2$  because the longitudinal momentum imparted

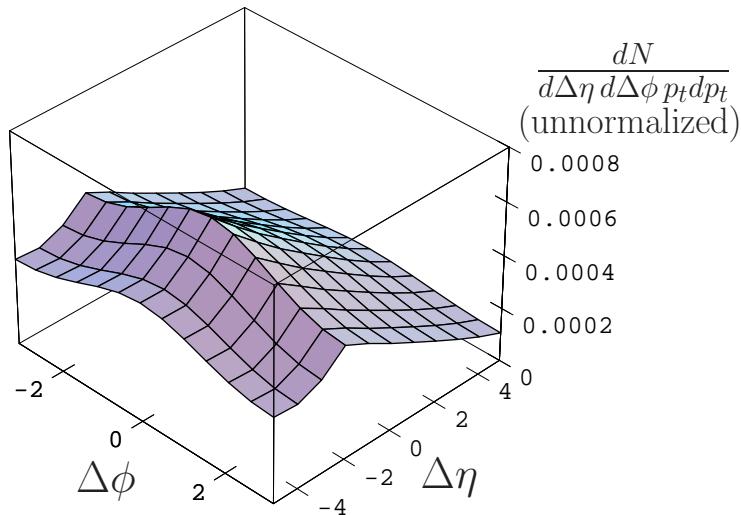


FIG. 8: The unnormalized yield  $dN/d\Delta\eta d\Delta\phi p_t dp_t$  of the associated particles as a function of  $\Delta\phi$  and  $\Delta\eta$  for a jet trigger of  $\eta = 3$ , calculated with the momentum kick model for  $p_t = 2$  GeV.

on the partons is limited and has a magnitude of only  $q = 0.8$  GeV, in the direction of the jet. This momentum kick shifts the parton longitudinal momentum of the partons only by about 0.8 unit, resulting in a  $\Delta\eta \sim -2.2$  relative to the incident jet of  $\eta_{jet} = 3$ .

Another question can be raised on the behavior of low- $p_t$  partons in the momentum kick model. We expect low- $p_t$  partons to be present at the moment of jet-parton collision and these partons can collide with the jet. Under the action of a momentum kick, the initial parton momentum is related to the final parton momentum by

$$\mathbf{p}_i = \mathbf{p}_f - q\mathbf{e}_{jet}. \quad (31)$$

For simplicity, we can focus our attention at final partons at  $(\Delta\phi_f, \Delta\eta_f) \sim (0, 0)$  with a trigger jet at  $\eta_{jet} \sim 0$ , as other kinematic regions can be similarly analyzed. Then, the magnitude of the initial parton transverse momentum is

$$p_{ti} = |p_{tf} - q|, \quad (32)$$

which has a minimum of zero at  $p_{tf} = q$  and it increases for  $p_{tf} > q$  and  $p_{tf} < q$ . In the momentum kick model, the final momentum distribution is given by the momentum distribution of the initial parton. One therefore expects that the final (observed) transverse momentum distribution of ridge particles has a peak at  $p_{ft} = q$ , decreasing on both sides for  $p_{tf} > q$  and  $p_{tf} < q$ . Because  $q$  has been found to have the value of 0.8 GeV, we therefore expect that the transverse momentum spectrum of ridge particles associated with the near-side jet will have a peak at  $p_{tf} \sim 0.8$  GeV at  $(\Delta\phi_f, \Delta\eta_f) \sim (0, 0)$ .

The above prediction of the momentum kick model is based on the idealization of parton-hadron duality for which the momentum and energy loss due to the action of picking up a sea quark or antiquark, or emitting a soft gluon, can be approximately neglected. For low  $p_t$  partons, these momentum and energy loss in the hadronization process may need to be corrected and accounted for, leading to modifications that will likely smear and shift the predicted peak of the transverse momentum distribution at  $p_{ft} \sim q$ . How the hadron-parton duality will be modified for these

low  $p_t$  partons will need to be investigated both experimentally and theoretically. In this connection, it is interesting to note that the experimental transverse spectra,  $dN/dp_t$ , of particles associated with the near-side jet in the low  $p_t$  region below 1 GeV in central collisions is relatively flat, in contrast distinction to the exponentially-increasing  $dN/dp_t$  spectrum of inclusive particles and the  $dN/dp_t$  spectrum of particles associated with the away-side jet, as shown in Fig. 3 of [1]. These data of particles associated with a near-side jet in [1] contain both the jet and the ridge components. It will be of great interest to separate out the near-side jet and the ridge components for low  $p_t$  associated particles, to see whether a ridge exists and whether there is any evidence of a momentum kick suffered by the initial partons in producing these observed hadrons with low transverse momenta.

## VIII. CONCLUSIONS AND DISCUSSIONS

The STAR Collaboration has observed a  $\Delta\phi$ - $\Delta\eta$  correlation of particles associated with a jet in RHIC collisions [1, 2, 3, 4, 5, 6]. The correlations can be decomposed into a near-side component as remnants of the trigger jet at  $(\Delta\phi, \Delta\eta) \sim (0, 0)$  and a ridge particle component at  $\Delta\phi \sim 0$  with a broad ridge structure in  $\Delta\eta$ . These two components have very different characteristics. The ridge particles bear the same “fingerprints” as those of inclusive particles, including their particle yields increasing with increasing participant numbers and having nearly similar temperatures. These characteristics suggest that the ridge particles originate from the same material of the produced partons of the dense medium, which later also materialize as inclusive particles.

The  $\Delta\phi \sim 0$  correlation of the ridge particles with the trigger jet suggests further that the ridge particles and the jet are related kinematically. It is therefore reasonable to propose the momentum kick model in which the ridge particles are identified as medium partons which suffer a collision with the jet and acquire a momentum kick along the jet direction. After the collided partons materialize as ridge particles and escape from the surface without additional collisions, they retain the collided parton final momentum distribution. The yield of the ridge particles associated with the jet therefore will depend on the momentum kick and the initial momentum distribution of the collided partons before the jet-parton collision.

To gain important insights into the ridge phenomenon, we idealize the momentum kick model by introducing as few parameters as possible. The relevant quantities are then the magnitude of the momentum kick  $q$  along the jet direction imparted by the jet to the collided parton, and the initial parton momentum distribution represented by the rapidity width parameter  $\sigma_y$  and the transverse momentum temperature  $T$ .

Under the action of a jet-parton momentum kick, a peak structure in  $\Delta\phi$  arises. For the same final parton transverse momentum  $p_{tf}$  and various  $\Delta\phi$  values, the jet-parton collision samples a smaller magnitude of initial parton transverse momentum  $p_{ti}$  at  $\Delta\phi = 0$  but it samples a larger magnitude of initial parton transverse momentum  $p_{ti}$  at  $\Delta\phi = \pi$ . As the initial transverse momentum distribution decreases rapidly with the initial transverse momentum  $p_{ti}$  as  $\exp\{-\sqrt{m^2 + p_{ti}^2}/T\}/m_{ti}$ , there are more collided partons at  $\Delta\phi = 0$  than at  $\Delta\phi = \pi$ , for the same observed final transverse momentum  $p_{tf}$ . The case of azimuthal angles between  $\Delta\phi = 0$  and  $\Delta\phi = \pi$  gives a momentum distribution in between these two limits, resulting in a peak structure in  $\Delta\phi$  centered at  $\Delta\phi = 0$ .

This width of the distribution along the  $\Delta\phi$  direction is sensitive to the magnitude of the momentum kick  $q$ . A small value of  $q$  will lead to a broad structure in  $\Delta\phi$ . A large value of  $q$  will lead to a narrow structure in  $\Delta\phi$ . The experimental data suggest a value of the momentum kick  $q$  of 0.8 GeV. As there is much that is not known about the non-perturbative properties of the medium and the collision processes, the experimental extraction of the jet-parton momentum kick provides useful information concerning the jet-parton collision and jet energy loss.

While the peak structure along the  $\Delta\phi$  direction at  $\Delta\phi = 0$  arises predominantly from the momentum kick, the ridge structure along the  $\Delta\eta$  direction in the  $\Delta\phi$ - $\Delta\eta$  plane on the other hand reflects the initial rapidity distribution  $dN/dy$  at the momentum of the jet-parton collision. Thus, if the momentum kick model is indeed the correct mechanism, the ridge structure associated with the near-side jet may be used to probe the parton momentum distribution at the moment of the jet-parton collision.

Previous measurements of inclusive particle rapidity distribution at RHIC for  $\sqrt{s_{NN}} = 200$  GeV gives a width parameter  $\sigma_y = 2.3$  which however leads to too steep a ridge slope in the momentum kick model to be favored by the experimental ridge distribution. The rapidity width  $\sigma_y \sim 5.5$  extracted from the momentum kick model appears to be greater than the rapidity width extracted from the inclusive particle rapidity distribution.

It is important to note that the rapidity width  $\sigma_y$  extracted from the momentum kick model measures the rapidity width  $\sigma_y$ (JPC) at the moment of the jet-parton collision, where JPC stands for “jet-parton collision”. The jet-parton collision occurs early in the nucleus-nucleus collision. The rapidity width  $\sigma_y$  measured by the inclusive particle distribution is the asymptotic rapidity width  $\sigma_y(t \rightarrow \infty)$  at the end point of the nucleus-nucleus collision.

Not much is known experimentally about the evolution of the rapidity distribution of partons as a function of time. Nevertheless, certain gross features can perhaps be inferred from general considerations, as depicted schematically in Fig. 9. At the onset of the nucleus-nucleus collision at  $t = 0$  in the collider frame, the partons have rapidity

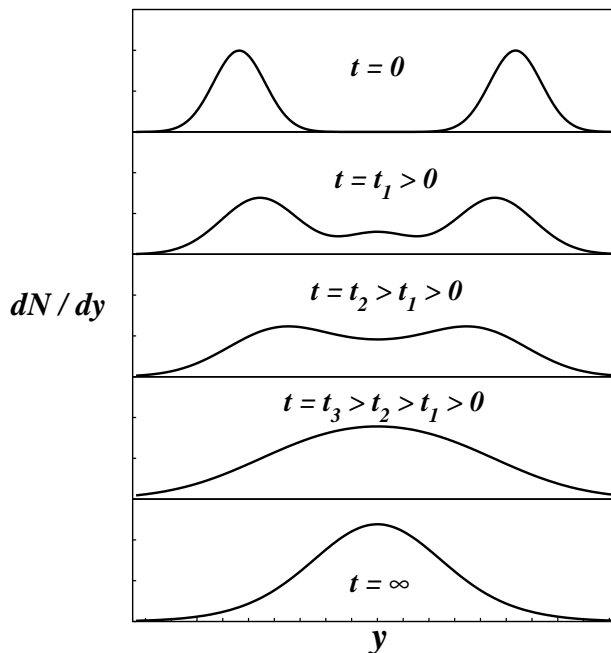


FIG. 9: Possible evolution scenario of the parton rapidity distribution  $dN/dy$  as a function of time.

distributions centered at the rapidities of the two colliding nuclei, each distribution having a rapidity width because of the fermi motion of the partons in the hadrons inside the nucleus. At a subsequent time  $t = t_1$ , the partons will thermalize and the rapidity distribution will evolve from a two-center distribution into an overlapping three-center distribution, with the thermalized component at zero rapidity (Fig. 9). The distributions on the two sides will move towards zero rapidity and will diminish their magnitudes, while the central distribution will gain in magnitude. The three-center distribution will eventually merge into a single distribution at times  $t = t_2$  and  $t = t_3$  in Fig. 9. In this scenario, the width  $\sigma_y(\text{JPC})$  should be larger than the asymptotic width  $\sigma_y(t \rightarrow \infty)$ , as the rapidity distribution at the moment of the jet-parton collision may only be in the early stage of the rapidity evolution from the two-center distribution to an overlapping three-center distribution and a merged single distribution. Because of the complicated dynamics that enters into the evolution of the early rapidity distribution, it is possible that the rapidity distribution at this stage may be non-Gaussian in shape. The determination of the full shape of the initial rapidity distribution will need the measurement of associated ridge particles at large values of  $|\Delta\eta|$ .

In conclusion, we find that the ridge structure in the  $\Delta\phi$ - $\Delta\eta$  correlation associated with a near-side jet [1, 2, 3, 4, 5, 6] can be explained in terms of the momentum kick model in which the ridge particles are identified as medium partons which suffer a collision with the jet and acquire a momentum kick along the jet direction. If this is indeed the correct mechanism, the near-side jet may be used to probe the parton momentum distribution at the moment of jet-parton collision, leading to the result that at that instant the parton temperature is slightly higher and the rapidity width substantially greater than corresponding quantities of their evolution products of inclusive particles at the end point of the nucleus-nucleus collision.

The author wishes to thank Drs. V. Cianciolo, J. Putschke, Fuqiang Wang, and Gang Wang for valuable communications and comments. The author also wishes to thank Drs. Huan Huang, C. Ogilvie, K. Read, and S. Sorensen for helpful discussions. This research was supported in part by the Division of Nuclear Physics, U.S. Department of Energy, under Contract No. DE-AC05-00OR22725, managed by UT-Battelle, LLC.

- 
- [1] J. Adams *et al.* for the STAR Collaboration, Phys. Rev. Lett. **95**, 152301 (2005).
  - [2] J. Adams *et al.* for the STAR Collaboration, Phys. Rev. C **73**, 064907 (2006).
  - [3] J. Putschke for the STAR Collaboration, Talk presented at presented at the 19th International Conference on Ultra-Relativistic Nucleus-Nucleus Collisions, "Quark Matter 2006", Shanghai, China, November 14-20, 2006, nucl-ex/0701074.
  - [4] J. Bielcikova for the STAR Collaboration, Talk presented at presented at the 19th International Conference on Ultra-Relativistic Nucleus-Nucleus Collisions, "Quark Matter 2006", Shanghai, China, November 14-20, 2006, nucl-ex/0701047.

- [5] J. Bielcikova for the STAR Collaboration, Talk presented at 23rd Winter Workshop on Nuclear Dynamics, Big Sky, Montana, USA, February 11-18, 2007, arXiv:0707.3100.
- [6] J. Longacre for the STAR Collaboration, Poster presented at presented at the 19th International Conference on Ultra-Relativistic Nucleus-Nucleus Collisions, "Quark Matter 2006", Shanghai, China, November 14-20, 2006, nucl-ex/0702008.
- [7] R. C. Hwa and C. B. Yang, Phys.Rev. C **67** 034902 (2003); R. C. Hwa and Z. G. Tan, Phys. Rev. C **72**, 057902 (2005); R. C. Hwa and C. B. Yang, nucl-th/0602024.
- [8] C. B. Chiu and R. C. Hwa Phys. Rev. C **72**, 034903 (2005).
- [9] P. Romatschke, Phys. Rev. C **75** 014901 (2007).
- [10] S. A. Voloshin, Nucl. Phys. **A749**, 287 (2005).
- [11] N. Armesto, C. A. Salgado, U. A. Wiedemann, Phys. Rev. Lett. **93**, 242301 (2004).
- [12] E. Shuryak, arXiv:0706.3531.
- [13] V. S. Pantuev, arXiv:0710.1882.
- [14] C. Y. Wong, *Introduction to High-Energy Heavy-Ion Collisions*, World Scientific Publisher, 1994.
- [15] M. Murray for the Brahms Collaboration, J. Phys. G. **30**, S667 (2004)
- [16] G. Wang and H. Huang, private communications.
- [17] L. Molnar for the STAR Collaboration, nucl-ex/0701061.
- [18] F. Wang for the STAR Collaboration, Invited talk at the XIth International Workshop on Correlation and Fluctuation in Multiparticle Production, Hangzhou, China, November 2007, arXiv:0707.0815.